Article

In Situ Synchrotron XRD Characterization of Piezoelectric $Al_{1-x}Sc_xN$ Thin Films for MEMS Applications

Wenzheng Jiang [1,2,†], Lei Zhu [1,2,†], Lingli Chen [1,2], Yumeng Yang [3], Xi Yu [4], Xiaolong Li [5], Zhiqiang Mu [1,2,*] and Wenjie Yu [1,2,*]

1 State Key Laboratory of Functional Materials for Informatics, Shanghai Institute of Microsystem and Information Technology, Chinese Academy of Sciences, Shanghai 200050, China
2 College of Materials Science and Opto-Electronic Technology, University of Chinese Academy of Sciences, Beijing 100049, China
3 Shanghai Engineering Research Center of Energy Efficient and Custom AI IC, School of Information Science and Technology, ShanghaiTech University, Shanghai 201210, China
4 School of Microelectronics, Shanghai University, Shanghai 200444, China
5 Shanghai Synchrotron Radiation Facility, Shanghai Institute of Applied Physics, Chinese Academy of Sciences, Shanghai 201204, China
* Correspondence: zqmu@mail.sim.ac.cn (Z.M.); casan@mail.sim.ac.cn (W.Y.)
† These authors contributed equally to this work.

Abstract: Aluminum scandium nitride ($Al_{1-x}Sc_xN$) film has drawn considerable attention owing to its enhanced piezoelectric response for micro-electromechanical system (MEMS) applications. Understanding the fundamentals of piezoelectricity would require a precise characterization of the piezoelectric coefficient, which is also crucial for MEMS device design. In this study, we proposed an in situ method based on a synchrotron X-ray diffraction (XRD) system to characterize the longitudinal piezoelectric constant d_{33} of $Al_{1-x}Sc_xN$ film. The measurement results quantitatively demonstrated the piezoelectric effect of $Al_{1-x}Sc_xN$ films by lattice spacing variation upon applied external voltage. The as-extracted d_{33} had a reasonable accuracy compared with the conventional high over-tone bulk acoustic resonators (HBAR) devices and Berlincourt methods. It was also found that the substrate clamping effect, leading to underestimation of d_{33} from in situ synchrotron XRD measurement while overestimation using Berlincourt method, should be thoroughly corrected in the data extraction process. The d_{33} of AlN and $Al_{0.9}Sc_{0.1}N$ obtained by synchronous XRD method were 4.76 pC/N and 7.79 pC/N, respectively, matching well with traditional HBAR and Berlincourt methods. Our findings prove the in situ synchrotron XRD measurement as an effective method for precise piezoelectric coefficient d_{33} characterization.

Keywords: aluminum scandium nitride; synchrotron XRD; piezoelectric coefficient; substrate clamping effect; micro-electromechanical system

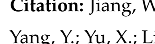

Citation: Jiang, W.; Zhu, L.; Chen, L.; Yang, Y.; Yu, X.; Li, X.; Mu, Z.; Yu, W. In Situ Synchrotron XRD Characterization of Piezoelectric $Al_{1-x}Sc_xN$ Thin Films for MEMS Applications. *Materials* **2023**, *16*, 1781. https://doi.org/10.3390/ma16051781

Academic Editor: Georgios C. Psarras

Received: 31 January 2023
Revised: 18 February 2023
Accepted: 20 February 2023
Published: 21 February 2023

Copyright: © 2023 by the authors. Licensee MDPI, Basel, Switzerland. This article is an open access article distributed under the terms and conditions of the Creative Commons Attribution (CC BY) license (https://creativecommons.org/licenses/by/4.0/).

1. Introduction

Recently, aluminum nitride (AlN) piezoelectric film has attracted great attention due to wireless communication technology experiencing rapid development from 2–4G to 5G [1]. Bulk acoustic wave (BAW) filters based on AlN piezoelectric film exhibit significant advantages in terms of compact size, high performance and high compatibility with the standard complementary metal-oxide-semiconductor (CMOS) process [2–4]. However, limited by the relatively low intrinsic longitudinal piezoelectric coefficient d_{33}, the bandwidths of BAW filters based on AlN piezoelectric film are generally less than 3% [5,6]. There is an urgent need to seek breakthroughs in AlN materials. Rare earth element doping, including scandium (Sc) [7–9], yttrium (Y) [10] and tantalum (Ta) [11], has been proven to be an effective method to improve the piezoelectric properties of AlN materials. Among them, scandium doping is regarded as the most efficient method, since Akiyama M demonstrated

a ~400% piezoelectric response increase in 2009 [7]. With the help of first-principle calculations, Tasnadi F [12] revealed that the increased intrinsic sensitivity of axial strain induced by large elastic softening leads to the anomalous enhancement of piezoelectric response by Sc introduction. For example, when the scandium concentration is 20%, the piezoelectric coefficient d_{33} of $Al_{0.8}Sc_{0.2}N$ film can increase from 5.38 pC/N to 11.19 pC/N, leading to a 9% relative bandwidth of the corresponding filters [13].

It is evident that the piezoelectric response of $Al_{1-x}Sc_xN$ film is a key parameter for the design and optimization of high-frequency acoustic resonators and filters. At present, $Al_{1-x}Sc_xN$ growth methods include magnetron sputtering, molecular beam epitaxy (MBE) [14] and metal-organic chemical vapor deposition (MOCVD) [15]. Among them, magnetron sputtering is still the most commonly used method for $Al_{1-x}Sc_xN$ piezoelectric material deposition due to its high compatibility with traditional device fabrication processes and relatively low manufacturing costs. Although the piezoelectric response of $Al_{1-x}Sc_xN$ film can be predicted by theoretical calculations [12,16], the values of fabricated films often deviate from the theoretical ones, due to the deterioration of crystalline quality, intrinsic stress and calculation accuracy. In particular, with the increase in Sc concentration to around 30%, the crystal quality of $Al_{1-x}Sc_xN$ film may significantly deteriorate because of abnormal oriented grains (AOG) formation. When Sc concentration is higher than 50%, the non-polar cubic structure is more stable than the polar wurtzite structure [16], which has adverse effects on its piezoelectric response [9,17–19]. Therefore, it is crucial to develop an effective and accurate experimental method for the evaluation of $Al_{1-x}Sc_xN$ film piezoelectric property.

At present, the methods commonly used for piezoelectric characterization include PiezoMeter [8], double-beam laser interferometry (DBLI) [20], piezoresponse force microscopy (PFM) [21] and acoustic resonators [22]. d_{33} values ranging from 3.2 pC/N to 4.53 pC/N were reported by using above methods [21,23,24], while slightly higher values ranging from 4.9 pC/N to 5.1 pC/N were obtained after measurement system calibration [25,26]. However, since the piezoelectric coefficient of $Al_{1-x}Sc_xN$ film is only tens of pC/N, about an order of magnitude smaller than barium titanate ($BaTiO_3$) [27] and zirconate titanate (PZT) [28], it is very challenging to characterize $Al_{1-x}Sc_xN$ film using these methods. Synchrotron radiation is an advanced collimated light source with a high intensity and a wide spectrum. X-ray diffraction (XRD) with an extremely powerful X-ray source produced by synchrotron radiation facilities offers a puissant and special technique by which to characterize the structure of materials on the atomic or molecular scales [29]. It provides greater accuracy to investigate material properties such as phase composition, crystallite size, strain and defect [30]. It also allows time-resolved in situ characterization with a significantly reduced measurement time and a much higher resolution, exhibiting particular advantages in structure characterization on sub-nanometer scales. For example, Shiomi et al. investigated the piezoelectric coefficient of $Al_{0.2}Ga_{0.8}N$ film based on synchrotron XRD, verifying the feasibility of this method to characterize the piezoelectric response at the picometer scale [31].

Herein, in the present work, we developed an in situ measurement system based on the synchrotron radiation-powered XRD technique to characterize the piezoelectric coefficient d_{33} of $Al_{1-x}Sc_xN$ films. The measured results quantitatively demonstrated the lattice spacing variation of $Al_{1-x}Sc_xN$ films induced by piezoelectric effect upon applied external voltage. Longitudinal piezoelectric coefficients d_{33} of $Al_{1-x}Sc_xN$ film with different Sc concentrations were successfully obtained and compared with traditional measurement methods. Moreover, by implementing substrate clamping effect calibration, the d_{33} deviation between synchrotron XRD and other methods was significantly reduced, indicating the validity of synchrotron XRD characterization for precise d_{33} measurement.

2. Materials and Methods

2.1. Synchrotron XRD Measurement System Setup

Figure 1a–c illustrates the brief fabrication process of $Al_{1-x}Sc_xN$ samples with x = 0, 10% and 20%. Firstly, 200 nm Mo/850 nm $Al_{1-x}Sc_xN$/150 nm Mo sandwiched stacks were deposited by magnetron reactive sputtering on high-resistivity Si substrate with a 30 nm AlN seed layer. Those three layers were continuously deposited without a vacuum break to avoid particle or photoresist residual contamination. Highly crystalline AlN film with (0002) the full width at half maximum (FWHM) of 1.40° was observed on controlled samples, while FWHM slightly increased to 1.76° and 2.90° for $Al_{0.9}Sc_{0.1}N$ and $Al_{0.8}Sc_{0.2}N$ film due to the deterioration of crystallinity caused by Sc introduction, as shown in Figure 2. Then, the top Mo layer was patterned using the ion beam etching (IBE) process and acted as a hard mask for subsequent $Al_{1-x}Sc_xN$-selective etching. Anisotropic etching of $Al_{1-x}Sc_xN$ films with different Sc contents was carried out by tetramethylammonium hydroxide (TMAH) for bottom mesa formation. Finally, top electrode Mo was patterned by IBE process for external voltage connection.

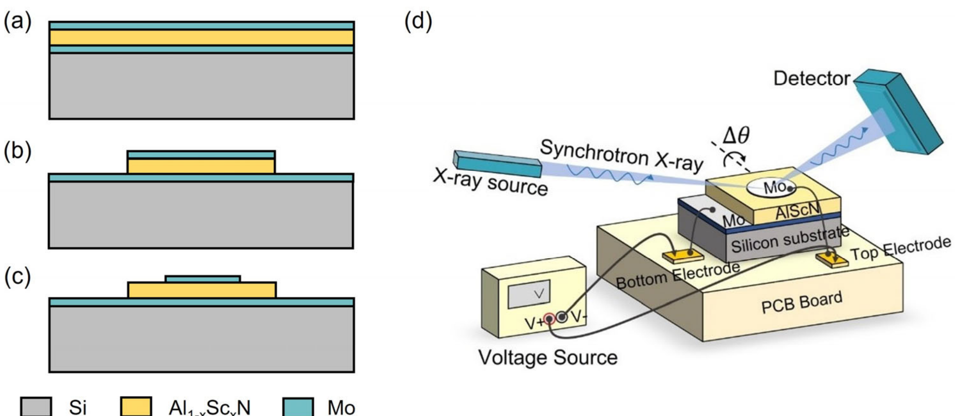

Figure 1. (**a**) Mo/$Al_{1-x}Sc_xN$/Mo piezoelectric stack deposition; (**b**) Top Mo/$Al_{1-x}Sc_xN$ etching; (**c**) Top electrode Mo patterning; (**d**) Schematic of the measurement setup for the in situ synchrotron XRD characterization under static voltage supply.

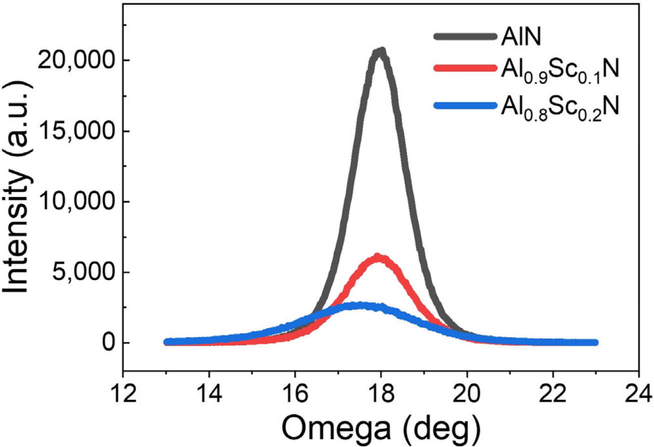

Figure 2. The XRD rocking curves of (0002) plane for AlN, $Al_{0.9}Sc_{0.1}N$ and $Al_{0.8}Sc_{0.2}N$.

The schematic of the in situ synchrotron XRD measurement system is shown in Figure 1d. It consists of a high-intensity X-ray source and detector, a printed circuit board and a voltage source. The previously fabricated $Al_{1-x}Sc_xN$ samples were mounted on the PCB board. The top and bottom electrodes were connected to the voltage source through lead bonding, which could effectively avoid the accidental penetration of piezoelectric film

in the testing process. The X-ray beam was incident at the center of the top electrode to obtain symmetric diffraction as external voltage was applied to the top electrodes of samples. The shift in synchrotron XRD curves could be observed by applying different voltages. Synchrotron XRD characterization was carried out at the Shanghai Synchrotron Radiation Light Source. The line stations used were BL14B1 and BL02U2, both of which can provide X-rays with an energy of 10 keV and support the in situ piezoelectric characterization of $Al_{1-x}Sc_xN$ samples.

2.2. High Overtone Bulk Acoustic Resonators Fabrication

High overtone bulk acoustic resonator (HBAR) devices, without the requirement of a suspended film structure, are widely used to estimate the piezoelectric response and electromechanical coupling coefficient with the advantage of a simplified fabrication process [32]. The fabrication process of $Al_{1-x}Sc_xN$ HBAR devices with x = 0 and 10% is shown in Figure 3. The essential piezoelectric stacks of an HBAR device, consisting of 200 nm Mo/850 nm $Al_{1-x}Sc_xN$/150 nm Mo sandwiched film stack, were continuously deposited on high-resistivity Si substrate with a 30 nm AlN seed layer, as shown in Figure 3a. The top Mo and $Al_{1-x}Sc_xN$ layers were etched by IBE and TMAH, respectively, as shown in Figure 3b. Benefiting from the highly selective and anisotropic TMAH etching, smooth and clean $Al_{1-x}Sc_xN$ sidewalls with a 50–60° etching profile were obtained, as shown in Figure 4. Due to the lower etching rate of $Al_{0.9}Sc_{0.1}N$ compared with pure AlN film, the sidewall angle of $Al_{0.9}Sc_{0.1}N$ was ~10° smaller with a tapered etching profile. It should be noted that the $Al_{1-x}Sc_xN$ film underneath the signal terminal of the top electrode should also be removed to avoid parasitic HBAR structure. Then, an oxide sidewall was formed at the boundary of the $Al_{1-x}Sc_xN$ etching area to avoid potential short circuit risk between the top and bottom electrodes (Figure 3c). Then, 20 nm Ti/300 nm Au was deposited and accordingly patterned for pad formation. Finally, the pentagonal-shaped top electrode was patterned to define the critical piezoelectric resonance area, as shown in Figure 3e. The frequency characteristics of the reflection coefficient (S_{11}) were carried out by a network analyzer KEYSIGHT E5071C.

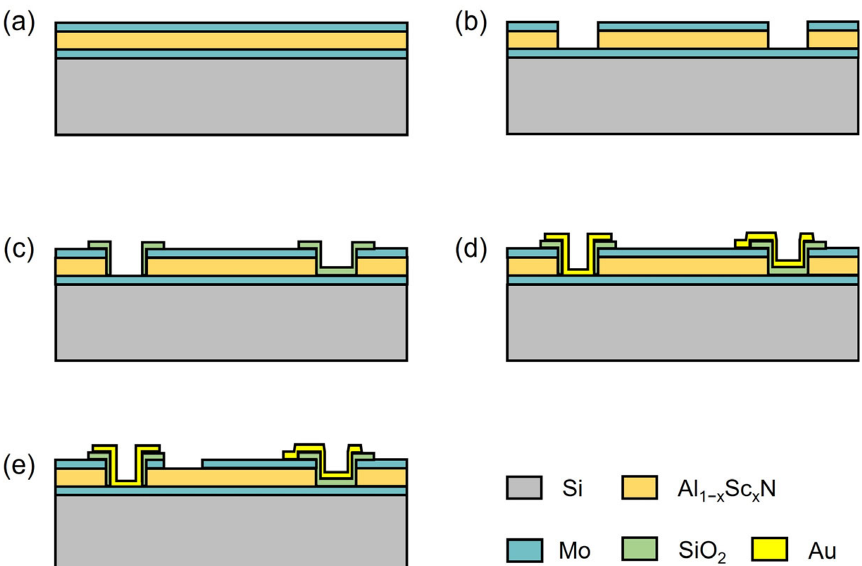

Figure 3. The fabrication process of $Al_{1-x}Sc_xN$ HBAR devices. (**a**) Mo/$Al_{1-x}Sc_xN$/Mo piezoelectric stack deposition, (**b**) Top Mo/$Al_{1-x}Sc_xN$ patterning, (**c**) SiO_2 isolation layer deposition and patterning, (**d**) Au contact layer deposition and patterning, (**e**) Top electrode Mo patterning.

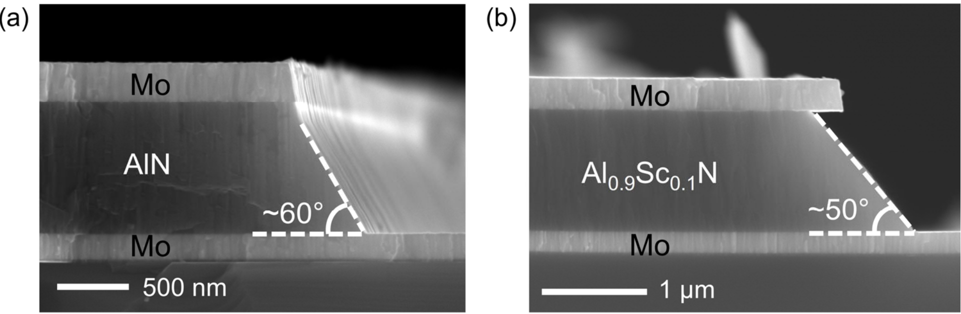

Figure 4. Cross-section SEM images of (**a**) AlN and (**b**) $Al_{0.9}Sc_{0.1}N$ piezoelectric stacks.

3. Results and Discussion

3.1. d_{33} Measurement by Synchrotron XRD Method

The in situ synchrotron XRD curves of AlN, $Al_{0.9}Sc_{0.1}N$ and $Al_{0.8}Sc_{0.2}N$ films under different applied voltages are shown in Figure 5. In general, the diffraction peaks of the $Al_{1-x}Sc_xN$ (0002) plane, reflecting the c-plane lattice spacing with different Sc concentrations and applied electric field, are located between 28.5° to 28.9°. As shown in Figure 5a, without external voltage, a distinct peak corresponding to AlN (0002) is located at 28.85°. A clear peak shift of 0.013° to lower angles was observed when a negative voltage of −100 V was applied; while an opposite 0.010° shift to higher angles was observed upon the application of positive 85 V. Synchrotron XRD curves of $Al_{1-x}Sc_xN$ films with Sc concentrations of 10% and 20% exhibit similar phenomena, with peak shifts of 0.010° and 0.015° for $Al_{0.9}Sc_{0.1}N$ and $Al_{0.8}Sc_{0.2}N$ films under applied voltages of 60 V and 40 V separately, as shown in Figure 5b,c. It should be emphasized that thanks to the high resolution of the synchrotron radiation-powered X-ray source, diffraction peak shifts as small as 0.001° can be clearly distinguished. This behavior corresponds to the inverse piezoelectric effect of piezoelectric film, and can in turn be used to calculate the piezoelectric coefficient. By applying a longitudinal electric field E on the piezoelectric films and calculating the change rate of (0002) interplanar spacing $(d_E – d_0)/d_0$, the longitudinal strain S and the piezoelectric coefficient d_{33} of piezoelectric films can be obtained according to Equation (1) [33]:

$$d_{33} = \left(\frac{\partial S_3}{\partial E_3}\right)^T = \frac{(d_E - d_0)}{d_0} \cdot \frac{1}{E}, \quad (1)$$

where d_E and d_0 are interplanar spacing with and without applied voltage. The interplanar spacing d is obtained by the classic Bragg formula $\lambda = 2dsin\theta$, where θ is the position of the diffraction peak. The energy of the synchrotron radiation-powered X-ray in the work is 10 keV, corresponding to a wavelength of 0.124 nm.

The obtained XRD curves were fitted using Gaussian functions to extract the 2θ values for the peaks, and the c-plane lattice spacing $d = \lambda/2sin\theta$ and longitudinal lattice strain $S = (d_E – d_0)/d_0$ were derived on the basis of the above equations. The applied electrical field dependence of the $Al_{1-x}Sc_xN$ strain is shown in Figure 5d–f. It is worth noting that the linear relationship between the applied external voltage and the lattice strain was observed, matching very well with the theoretical piezoelectric effect of $Al_{1-x}Sc_xN$ films. The d_{33} can be obtained by extracting the slop from the strain—electrical field correlations. The d_{33} of pure AlN film is extracted at 3.54 pm/V. When the scandium concentration increases to 10% and 20%, the d_{33} increases to 5.58 pm/V and 9.48 pm/V, corresponding to a 57.6% and a 168% improvement, respectively.

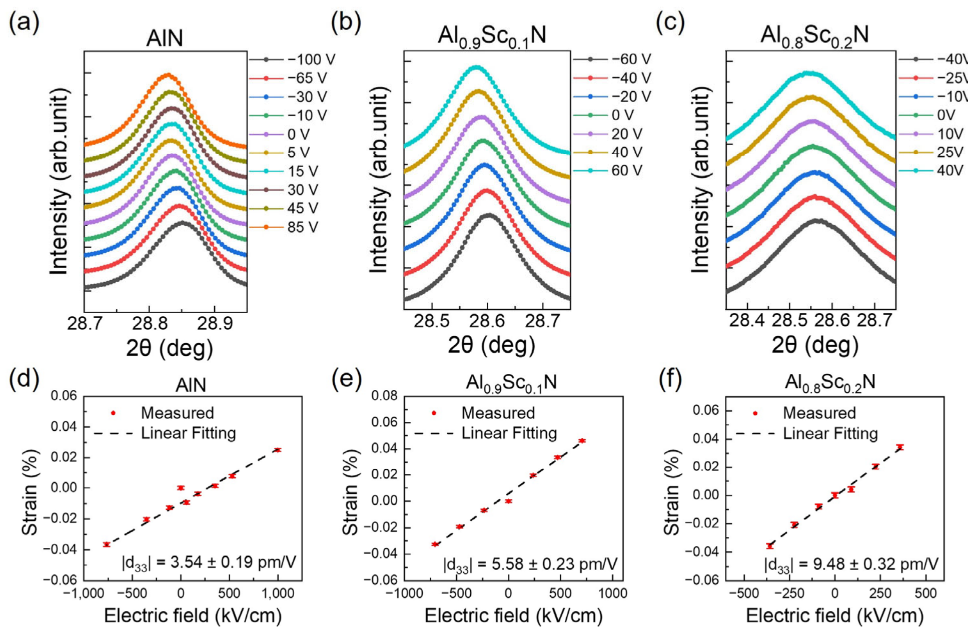

Figure 5. Synchrotron XRD curves of (**a**) AlN, (**b**) $Al_{0.9}Sc_{0.1}N$, (**c**) $Al_{0.8}Sc_{0.2}N$ under different applied voltages V; Electric field E dependence of longitudinal strains of (**d**) AlN, (**e**) $Al_{0.9}Sc_{0.1}N$, (**f**) $Al_{0.8}Sc_{0.2}N$ derived from synchrotron XRD peaks. The data from the standard PDF cards for AlN (No. 00-025-1133) are referred.

3.2. d_{33} Measurement by HBAR Method

As a comparison, we also adopted the commonly used acoustic resonators for d_{33} characterization. Figure 6a shows the top-view SEM image of the fabricated $Al_{1-x}Sc_xN$ HBAR device with a pentagon-shaped resonant area. As shown in Figure 6b, the S_{11} curves of $Al_{1-x}Sc_xN$ HBAR devices with Sc concentrations of 0% and 10% exhibit multiple resonance modes in the measured frequency range. The strongest resonance frequency is located around 3.00 GHz and 2.58 GHz, with 10.04 MHz and 9.90 MHz frequencies splitting between adjacent modes for AlN and $Al_{0.9}Sc_{0.1}N$ films, respectively.

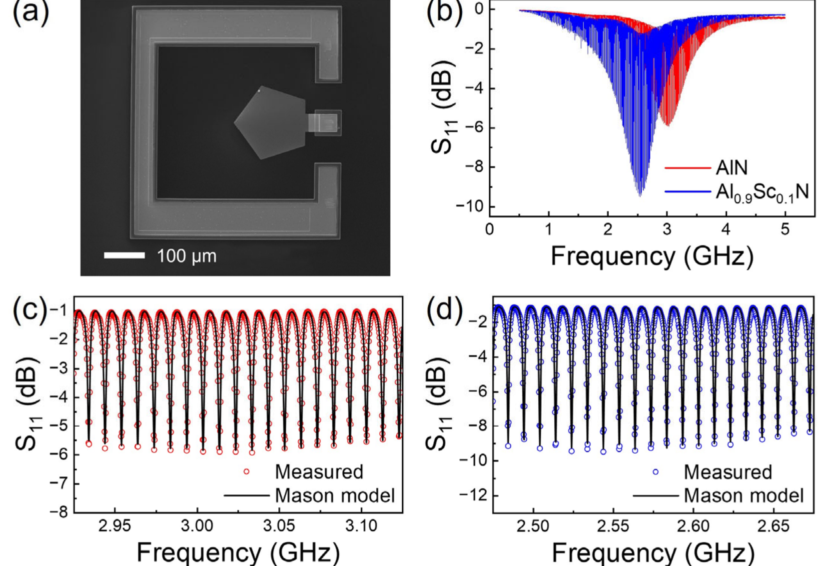

Figure 6. (**a**) Top-view SEM image of $Al_{1-x}Sc_xN$ HBAR device; (**b**) S_{11} response of HBAR devices with AlN and $Al_{0.9}Sc_{0.1}N$ films; Mason equivalent circuit fitting of (**c**) AlN and (**d**) $Al_{0.9}Sc_{0.1}N$ on a 200 MHz span.

Mason models incorporated with measured scattering curves are commonly adopted for material parameter extraction [34]. The equivalent circuit of a Mason model for $Al_{1-x}Sc_xN$ HBAR devices, consisting of an Si substrate, a bottom electrode, a piezoelectric layer and a top electrode, is shown in Figure 7; where Z, γ, C_0 are acoustic impedance, phase shift and static capacitance, respectively. $h = e/\varepsilon^S$, where e is the relevant components of the piezoelectric matrix, and ε^S is the permittivity of piezoelectric materials. As shown in Figure 6c,d, the simulated results of the Mason model are in good agreement with the measured S_{11} curves. The d_{33} of AlN and $Al_{0.9}Sc_{0.1}N$ films extracted using the Mason model are 4.22 pC/N and 6.04 pC/N, respectively.

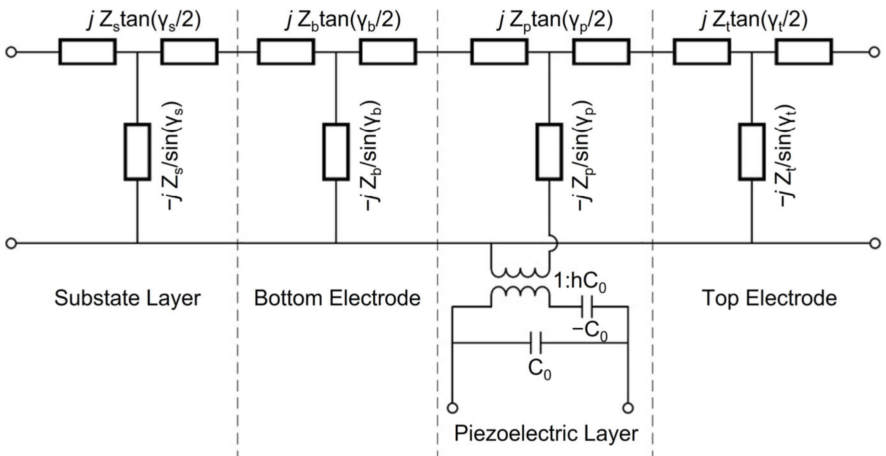

Figure 7. Equivalent circuit of the Mason model for $Al_{1-x}Sc_xN$ HBAR device.

3.3. *d_{33} Measurement by PM300 Method*

Figure 8a illustrates d_{33} measurements using the Berlincourt method PIEZOTEST PM300 [35,36]. $Al_{1-x}Sc_xN$ piezoelectric samples were clamped between two contact probes and subjected to a low frequency force. Electrical signals generated from $Al_{1-x}Sc_xN$ film were collected and compared with a built-in reference, and thus d_{33} values with polarization direction could be directly given by the system. As for $Al_{1-x}Sc_xN$ sample preparation, 900 nm $Al_{1-x}Sc_xN$ films with x = 0% and 10% were directly deposited on low resistivity Si substrates. Then, a 250 nm Au top electrode was deposited and patterned for top electrical connection, as shown in Figure 8b. The d_{33} values of AlN and $Al_{0.9}Sc_{0.1}N$ films measured by PIEZOTEST PM300 were 6.33 pC/N and 8.96 pC/N, respectively.

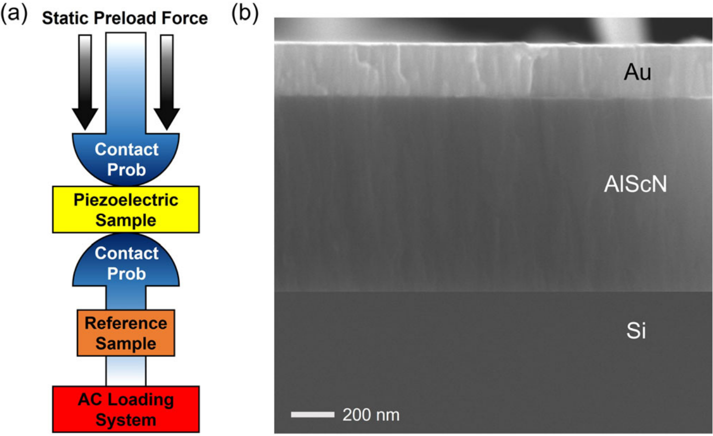

Figure 8. (**a**) Schematic of d_{33} measurement by PIEZOTEST PM300 [36]; (**b**) Cross-section SEM image of piezoelectric sample.

3.4. d_{33} Discussion

The piezoelectric coefficient d_{33} of AlN and $Al_{0.9}Sc_{0.1}N$ films measured by Synchrotron XRD, HBAR and PIEZOTEST PM300, together with theoretical calculated values, are summarized in Table 1. The theoretical calculations were performed using the Vienna Ab initio Simulation Package (VASP) [37–39]. It is observed that the d_{33} measured by synchrotron XRD are about 40% lower compared to that measured by PM300, while the d_{33} values obtained by synchrotron XRD and HBAR are much closer (~10%). Moreover, compared with theoretical values, the measured results from synchrotron XRD and HBAR are 22–34% smaller, while that of PM300 are 14-18% larger. One possible reason for the above deviations may come from measurement system errors, fabrication process variations and crystalline quality differences in the piezoelectric film. However, this alone is not reasonable to explain such consistently large deviations introduced by each method, and needs to be carefully considered.

Table 1. The measured and corrected d_{33} of AlN and $Al_{0.9}Sc_{0.1}N$ films from synchrotron XRD, PM300, HBAR and theoretical calculation.

Material	Method	Measured d_{33} (pC/N)	Corrected d_{33} (pC/N)	Theoretical Calculated d_{33} (pC/N)
AlN	Synchrotron XRD	3.54	4.76	5.38
	PM300	6.33	4.29	
	HBAR	4.22	5.43	
$Al_{0.9}Sc_{0.1}N$	Synchrotron XRD	5.58	7.79	7.89
	PM300	8.96	7.03	
	HBAR	6.04	8.25	

Since the deformation amount of $Al_{1-x}Sc_xN$ piezoelectric film is relatively small (only tens of picometers/voltage), the influence of the rigid substrate clamped to the piezoelectric film cannot be ignored during d_{33} measurement. Referring to Lefki et al. [40], the interference of the substrate during d_{33} measurement is quantitatively analyzed below.

The following equations can be deduced from the classic piezoelectric equation based on the symmetry of $Al_{1-x}Sc_xN$ materials [40]:

$$D_3 = d_{31}\cdot(T_1 + T_2) + d_{33}\cdot T_3 + \varepsilon_{33}^T\cdot E_3, \tag{2}$$

$$S_1 = s_{11}^E\cdot T_1 + s_{12}^E\cdot T_2 + s_{13}^E\cdot T_3 + d_{31}\cdot E_3, \tag{3}$$

$$S_2 = s_{12}^E\cdot T_1 + s_{11}^E\cdot T_2 + s_{13}^E\cdot T_3 + d_{31}\cdot E_3, \tag{4}$$

$$S_3 = s_{13}^E\cdot T_1 + s_{13}^E\cdot T_2 + s_{33}^E\cdot T_3 + d_{33}\cdot E_3, \tag{5}$$

where D_3 is the longitudinal electrical displacement of the piezoelectric film, S_1, S_2, S_3 and T_1, T_2, T_3 are the strain and stress of the film in the in-plane x, y and out-of-plane z directions, respectively, d_{31} is the transverse piezoelectric coefficient, ε_{33}^T is the dielectric constant of the film in the longitudinal direction, and s_{11}^E, s_{12}^E, s_{13}^E, s_{33}^E are the mechanical compliances of the piezoelectric film.

As described above, synchrotron XRD uses the inverse piezoelectric effect for d_{33} measurement. Ideally, the piezoelectric film would deform both in the longitudinal and in-plane directions when the voltage is applied. However, due to the restrictions from the substrate, the in-plane strains of piezoelectric film in the x and y direction S_1 and S_2 are assumed as zero. Since the longitudinal stress $T_3 = 0$, the in-plain stress can be deduced from Equations (3) and (4) as:

$$T_1 = T_2 = \frac{-d_{31}E_3}{s_{11}^E + s_{12}^E} \tag{6}$$

The calibrated longitudinal piezoelectric coefficient $d_{33,i}$ considering inverse piezoelectric effect can be expressed as:

$$d_{33,i} = \frac{\Delta l}{V} = \frac{S_3}{E_3} = d_{33,\text{XRD}} + \frac{2s_{13}^E d_{31}}{s_{11}^E + s_{12}^E} \tag{7}$$

where $d_{33,\text{XRD}}$ is the experimental result measured by synchrotron XRD. By using theoretical values of s_{11}^E, s_{12}^E, s_{13}^E and d_{31} for a rough evaluation, the measured $d_{33,\text{XRD}}$ from synchrotron XRD is underestimated because of the deformation constraint by the substrate. The d_{33} value of AlN and $Al_{0.9}Sc_{0.1}N$ films obtained by synchronous XRD is revised to 4.76 pC/N and 7.79 pC/N according to above the correction, which is 34% and 40% larger than the originals.

The d_{33} extracted using the HBAR device also uses the inverse piezoelectric effect, which is similar to synchrotron XRD. The calibrated $d_{33,r}$ can be expressed by replacing the flexibility coefficient s_{ij}^E and piezoelectric strain coefficient d_{ij} in Equation (7) with the stiffness coefficient C_{ij}^E and piezoelectric stress coefficient e_{ij}, as shown below:

$$s_{11}^E = \frac{C_{11}^E C_{33}^E - C_{13}^{E\,2}}{\left(C_{11}^E - C_{12}^E\right)\left[c_{33}^E\left(C_{11}^E + C_{12}^E\right) - 2C_{13}^{E\,2}\right]}, \tag{8}$$

$$s_{12}^E = -\frac{C_{12}^E C_{33}^E - C_{13}^{E\,2}}{\left(C_{11}^E - C_{12}^E\right)\left[c_{33}^E\left(C_{11}^E + C_{12}^E\right) - 2C_{13}^{E\,2}\right]}, \tag{9}$$

$$s_{13}^E = -\frac{C_{13}^E}{c_{33}^E\left(C_{11}^E + C_{12}^E\right) - 2C_{13}^{E\,2}}, \tag{10}$$

$$d_{31} = \frac{e_{31} C_{33}^E - e_{33} C_{13}^E}{\left(C_{11}^E + C_{12}^E\right) C_{33}^E - 2C_{12}^{E\,2}}, \tag{11}$$

$$d_{33} = \frac{e_{33}\left(C_{11}^E + C_{12}^E\right) - 2e_{31} C_{13}^E}{\left(C_{11}^E + C_{12}^E\right) C_{33}^E - 2C_{13}^{E\,2}}. \tag{12}$$

$d_{33,r}$ extracted from HBAR devices can be expressed as:

$$d_{33,r} = \frac{e_{33}}{C_{33}^E}. \tag{13}$$

According to the above, the $d_{33,r}$ of the AlN and $Al_{0.9}Sc_{0.1}N$ films is revised to 5.43 pC/N and 8.25 pC/N, leading to a 29% and 37% increase from the originals. It is observed that the revised piezoelectric coefficient d_{33} obtained by HBAR devices is consistent with that from synchrotron XRD.

Although the Berlincourt method is the most convenient and fast way for piezoelectric coefficient measurement, the substrate would deform in-plane alongside $Al_{1-x}Sc_xN$ film due to the Poisson effect, introducing additional in-plane strain in piezoelectric films. The relationship between strain, Poisson's ratio μ and Young's modulus of substrate Y can be expressed as:

$$S_1 = S_2 = -\frac{\mu T_3}{Y} \tag{14}$$

Then, the in-plane stress is straightforwardly calculated from the strain-stress equation as follows:

$$T_1 = T_2 = \frac{-\frac{\mu T_3}{Y} - d_{31} E_3 - s_{13}^E T_3}{s_{11}^E + s_{12}^E} \tag{15}$$

The calibrated longitudinal piezoelectric coefficient $d_{33,d}$ considering the substrate-restricted direct piezoelectric effect can be expressed as:

$$d_{33,d} = \frac{Q}{F_3} = \frac{D_3}{T_3} = d_{33,\mathrm{PM300}} + 2d_{31}\frac{\frac{\mu}{Y} + s_{13}^E}{s_{11}^E + s_{12}^E}, \tag{16}$$

where $d_{33,\mathrm{PM300}}$ is the experimental result measured by PM300. $2d_{31}\frac{\frac{\mu}{Y}+s_{13}^E}{s_{11}^E+s_{12}^E}$ in Equation (16) is negative for $Al_{1-x}Sc_xN$ film due to additional in-plane stress, leading to an overestimated $d_{33,\mathrm{PM300}}$ measurement results. The d_{33} of AlN and $Al_{0.9}Sc_{0.1}N$ films obtained by PM300 is thus revised to 4.29 pC/N and 7.03 pC/N from 6.33 pC/N and 8.96 pC/N. It should be noted that the actual measurement process is much more complex due to the influence of the substrate's resistivity, quasi-static external force and fixed clamping force during PM300 measurement.

Table 1 summarizes the d_{33} results of synchrotron XRD, PM300 and HBAR before and after substrate-related calibration. The revised d_{33} value of synchrotron XRD is 34–40% higher, while the value of PM300 is 22–32% lower compared with the original values. As a result, the deviation obtained by these two methods is reduced from up to 70% to about 10%. The deviation between the synchrotron XRD and HBAR results is within 15%, and the deviation between synchrotron XRD and theoretical values is within 13%, which is believed to be caused by the crystalline quality, sample structure and measurement configurations [41]. Moreover, the d_{33} value of $Al_{0.9}Sc_{0.1}N$ films is consistent in the range of 7.03 pC/N to 8.25 pC/N obtained by different methods, which is always 52–64% higher than pure AlN. This is consistent with previous reports [8,16,42], indicating that Sc introduction can significantly improve the intrinsic piezoelectric property of AlN film. The d_{33} values obtained using the synchrotron XRD method are also in good agreement with previously reported results, as shown in Table 2. The above results demonstrate the feasibility and effectiveness of the synchrotron XRD method and the applicability of the proposed revised models.

Table 2. d_{33} comparison with other reports.

Material	d_{33} (pC/N)	Reference	Material	d_{33} (pC/N)	Reference
AlN	4.53	[24]	$Al_{0.9}Sc_{0.1}N$	7.5	[8]
AlN	4.76	Our work	$Al_{0.9}Sc_{0.1}N$	7.79	Our work
AlN	4.9	[25]	$Al_{0.88}Sc_{0.12}N$	7.9	[43]
AlN *	5.0	[44]	$Al_{0.85}Sc_{0.15}N$	7.92	[22]
AlN	5.1	[26]	$Al_{0.83}Sc_{0.17}N$	9.5	[43]
AlN *	5.1	[45]	$Al_{0.8}Sc_{0.2}N$	11.5	[8]
AlN	5.53	[46]	$Al_{0.75}Sc_{0.25}N$	13.2	[47]

* Obtained by theoretical calculations.

The Berlincourt method is predominantly used for d_{33} measurement due to its simple and quick measurement process. However, it is very difficult to produce a homogeneous uniaxial stress on the piezoelectric film, and the results may be affected by the sample clamping situation and electrode size; therefore, the method is usually suggested for d_{33} relative comparison [48]. The HBAR method can be not only used for d_{33} measurement, but also for a complete set of material parameters, such as the dielectric constant, sound velocity and density [49]. However, it requires a complete fabrication process of acoustic devices, and the results strongly depend on the accuracy of the resonance frequencies and the fitting precision of a large group of material parameters. Compared with the HBAR method, the sample fabrication process of synchrotron XRD is much simpler. What is more, though a few theoretical parameters are used during substrate clamping effect calibration, the d_{33} is directly extracted from the strain—electric field correlation without the involvement of material parameters, and the accuracy of the obtained results can also be roughly verified by the linearity of the strain—electric field relation.

4. Conclusions

In summary, synchrotron XRD, together with HBAR devices and a PM300 PiezoMeter, was adopted to accurately characterize the longitudinal piezoelectric coefficient (d_{33}) of $Al_{1-x}Sc_xN$ films in this paper. By considering the substrate clamping effect, more reliable and consistent d_{33} results were obtained, exhibiting the indispensability of the correction metlongitudinal piezoelectric coefficient hod for piezoelectric characterization, especially for materials with a small piezoelectric coefficient, such as the $Al_{1-x}Sc_xN$ system. Moreover, synchrotron XRD was proven as an effective method by which to evaluate the accuracy of d_{33} extracted from PIEZOTEST PM300 and HBAR, providing a feasible, precise and alternative technique for piezoelectric response characterization.

Author Contributions: Data curation, W.J., L.Z., L.C. and X.Y.; Formal analysis, W.J.; Funding acquisition, L.Z. and Z.M.; Investigation, W.J.; Project administration, L.Z.; Resources, X.L.; Software, X.Y.; Supervision, W.Y.; Validation, Z.M. and W.Y.; Writing—original draft, W.J.; Writing—review and editing, Y.Y. and Z.M. All authors have read and agreed to the published version of the manuscript.

Funding: This research was funded by the National Natural Science Foundation of China, grant No. 62274171, the Natural Science Foundation of Shanghai, grant No. 21ZR1474500 and Shanghai Technology Innovation Project, grant Nos. 20DZ1100603 and 22501100700.

Institutional Review Board Statement: Not applicable.

Informed Consent Statement: Not applicable.

Data Availability Statement: The data presented in this study are available on request from the corresponding author.

Conflicts of Interest: The authors declare no conflict of interest.

References

1. Ruby, R. A Snapshot in Time: The Future in Filters for Cell Phones. *IEEE Microw. Mag.* **2015**, *16*, 46–59. [CrossRef]
2. Weigel, R.; Morgan, D.P.; Owens, J.M.; Ballato, A.; Lakin, K.M.; Hashimoto, K.; Ruppel, C.C.W. Microwave acoustic materials, devices, and applications. *IEEE Trans. Microw. Theory Tech.* **2002**, *50*, 738–749. [CrossRef]
3. Aigner, R. SAW and BAW technologies for RF filter applications: A review of the relative strengths and weaknesses. In Proceedings of the 2008 IEEE Ultrasonics Symposium, Beijing, China, 2–5 November 2008; pp. 582–589. [CrossRef]
4. Ruby, R.C.; Bradley, P.; Oshmyansky, Y.; Chien, A.; Larson, J.D. Thin film bulk wave acoustic resonators (FBAR) for wireless applications. In Proceedings of the 2001 IEEE Ultrasonics Symposium, Atlanta, GA, USA, 7–10 October 2001; pp. 813–821. [CrossRef]
5. Liu, Y.; Cai, Y.; Zhang, Y.; Tovstopyat, A.; Liu, S.; Sun, C. Materials, Design, and Characteristics of Bulk Acoustic Wave Resonator: A Review. *Micromachines* **2020**, *11*, 630. [CrossRef]
6. Aigner, R.; Fattinger, G.; Schaefer, M.; Karnati, K.; Rothemund, R.; Dumont, F. BAW Filters for 5G Bands. In Proceedings of the 2018 IEEE International Electron Devices Meeting, San Francisco, CA, USA, 1–5 December 2018; pp. 14.15.11–14.15.14. [CrossRef]
7. Akiyama, M.; Kamohara, T.; Kano, K.; Teshigahara, A.; Takeuchi, Y.; Kawahara, N. Enhancement of piezoelectric response in scandium aluminum nitride alloy thin films prepared by dual reactive cosputtering. *Adv. Mater.* **2009**, *21*, 593–596. [CrossRef]
8. Akiyama, M.; Kano, K.; Teshigahara, A. Influence of growth temperature and scandium concentration on piezoelectric response of scandium aluminum nitride alloy thin films. *Appl. Phys. Lett.* **2009**, *95*, 162107. [CrossRef]
9. Akiyama, M.; Umeda, K.; Honda, A.; Nagase, T. Influence of scandium concentration on power generation figure of merit of scandium aluminum nitride thin films. *Appl. Phys. Lett.* **2013**, *102*, 021915. [CrossRef]
10. Mayrhofer, P.M.; Riedl, H.; Euchner, H.; Stöger-Pollach, M.; Mayrhofer, P.H.; Bittner, A.; Schmid, U. Microstructure and piezoelectric response of $Y_xAl_{1-x}N$ thin films. *Acta Mater.* **2015**, *100*, 81–89. [CrossRef]
11. Liu, H.; Zeng, F.; Tang, G.; Pan, F. Enhancement of piezoelectric response of diluted Ta doped AlN. *Appl. Surf. Sci.* **2013**, *270*, 225–230. [CrossRef]
12. Tasnadi, F.; Alling, B.; Hoglund, C.; Wingqvist, G.; Birch, J.; Hultman, L.; Abrikosov, I.A. Origin of the anomalous piezoelectric response in wurtzite $Sc_xAl_{1-x}N$ alloys. *Phys. Rev. Lett.* **2010**, *104*, 137601. [CrossRef] [PubMed]
13. Wang, J.L.; Park, M.; Mertin, S.; Pensala, T.; Ayazi, F.; Ansari, A. A Film Bulk Acoustic Resonator Based on Ferroelectric Aluminum Scandium Nitride Films. *J. Microelectromech. Syst.* **2020**, *29*, 741–747. [CrossRef]
14. Ansari, A. Single Crystalline Scandium Aluminum Nitride: An Emerging Material for 5G Acoustic Filters. In Proceedings of the 2019 IEEE MTT-S International Wireless Symposium (IWS), Guangzhou, China, 19–22 May 2019; pp. 1–3. [CrossRef]

15. Leone, S.; Ligl, J.; Manz, C.; Kirste, L.; Fuchs, T.; Menner, H.; Prescher, M.; Wiegert, J.; Žukauskaitė, A.; Quay, R.; et al. Metal-Organic Chemical Vapor Deposition of Aluminum Scandium Nitride. *Phys. Status. Solidi. Rapid. Res. Lett.* **2019**, *14*, 1900535. [CrossRef]
16. Momida, H.; Teshigahara, A.; Oguchi, T. Strong enhancement of piezoelectric constants in $Sc_xAl_{1-x}N$: First-principles calculations. *AIP Adv.* **2016**, *6*, 065006. [CrossRef]
17. Mertin, S.; Pashchenko, V.; Parsapour, F.; Sandu, C.S.; Heinz, B.; Rattunde, O.; Christmann, G.; Dubois, M.-A.; Muralt, P. Enhanced piezoelectric properties of c-axis textured aluminium scandium nitride thin films with high scandium content: Influence of intrinsic stress and sputtering parameters. In Proceedings of the 2017 IEEE International Ultrasonics Symposium, Washington, DC, USA, 6–9 September 2017; p. 1. [CrossRef]
18. Sandu, C.S.; Parsapour, F.; Mertin, S.; Pashchenko, V.; Matloub, R.; LaGrange, T.; Heinz, B.; Muralt, P. Abnormal Grain Growth in AlScN Thin Films Induced by Complexion Formation at Crystallite Interfaces. *Phys. Status Solidi A* **2019**, *216*, 1800569. [CrossRef]
19. Mertin, S.; Heinz, B.; Rattunde, O.; Christmann, G.; Dubois, M.A.; Nicolay, S.; Muralt, P. Piezoelectric and structural properties of c-axis textured aluminium scandium nitride thin films up to high scandium content. *Surf. Coat. Tech.* **2018**, *343*, 2–6. [CrossRef]
20. Shetty, S.; Yang, J.I.; Stitt, J.; Trolier-McKinstry, S. Quantitative and high spatial resolution d_{33} measurement of piezoelectric bulk and thin films. *J. Appl. Phys.* **2015**, *118*, 174104. [CrossRef]
21. Rodriguez, B.J.; Kim, D.J.; Kingon, A.I.; Nemanich, R.J. Measurement of the Effective Piezoelectric Constant of Nitride Thin Films and Heterostructures Using Scanning Force Microscopy. *Mat. Res. Soc. Symp. Proc.* **2011**, *693*, 798–803. [CrossRef]
22. Moreira, M.; Bjurstrom, J.; Katardjev, I.; Yantchev, V. Aluminum scandium nitride thin-film bulk acoustic resonators for wide band applications. *Vacuum* **2011**, *86*, 23–26. [CrossRef]
23. Sivaramakrishnan, S.; Mardilovich, P.; Schmitz-Kempen, T.; Tiedke, S. Concurrent wafer-level measurement of longitudinal and transverse effective piezoelectric coefficients ($d_{33,f}$ and $e_{31,f}$) by double beam laser interferometry. *J. Appl. Phys.* **2018**, *123*, 014103. [CrossRef]
24. Bu, G.; Ciplys, D.; Shur, M.; Schowalter, L.J.; Schujman, S.; Gaska, R. Electromechanical coupling coefficient for surface acoustic waves in single-crystal bulk aluminum nitride. *Appl. Phys. Lett.* **2004**, *84*, 4611–4613. [CrossRef]
25. Mcneil, L.E.; Grimsditch, M.; French, R.H. Vibrational Spectroscopy of Aluminum Nitride. *J. Am. Ceram. Soc.* **1993**, *76*, 1132–1136. [CrossRef]
26. Tsubouchi, K.; Sugai, K.; Mikoshiba, N. AlN Material Constants Evaluation and SAW Properties on AlN/Al_2O_3 and AlN/Si. In Proceedings of the 1981 Ultrasonics Symposium, Chicago, IL, USA, 14–16 October 1981; pp. 375–380. [CrossRef]
27. Tazaki, R.; Fu, D.; Itoh, M.; Daimon, M.; Koshihara, S.Y. Lattice distortion under an electric field in $BaTiO_3$ piezoelectric single crystal. *J. Phys. Condens. Matter* **2009**, *21*, 215903. [CrossRef] [PubMed]
28. Tan, G.; Maruyama, K.; Kanamitsu, Y.; Nishioka, S.; Ozaki, T.; Umegaki, T.; Hida, H.; Kanno, I. Crystallographic contributions to piezoelectric properties in PZT thin films. *Sci. Rep.* **2019**, *9*, 7309. [CrossRef] [PubMed]
29. Biger, H.; Degnah, A.; Salur, E.; Svkliyildiz, L.; Tsakalakos, T.; Akdogan, E.K. Multicycle flash sintering of cubic Y_2O_3-stabilized ZrO_2: An in situ energy dispersive synchrotron x-ray diffraction study with high temporal resolution. *Mater. Today. Commun.* **2022**, *33*, 104272. [CrossRef]
30. ŞAvkliyildiz, İ. In-Situ Strain Measurement on Al7075 Plate by Using High Energy Synchrotron Light Source. *Eur. J. Lipid. Sci. Tech.* **2021**, *23*, 435–439. [CrossRef]
31. Shiomi, H.; Ueda, A.; Tohei, T.; Imai, Y.; Hamachi, T.; Sumitani, K.; Kimura, S.; Ando, Y.; Hashizume, T.; Sakai, A. Analysis of inverse-piezoelectric-effect-induced lattice deformation in AlGaN/GaN high-electron-mobility transistors by time-resolved synchrotron radiation nanobeam X-ray diffraction. *Appl. Phys. Express* **2021**, *14*, 095502. [CrossRef]
32. Soutome, T.; Yanagitani, T. A method to estimate kt^2 of piezoelectric films from the change of lattice strain by XRD without removing substrate. In Proceedings of the 2019 IEEE International Ultrasonics Symposium, Glasgow, UK, 6–9 October 2019; pp. 301–304. [CrossRef]
33. *ANSI/IEEE Std 176-1987*; IEEE Standard on Piezoelectricity. IEEE: New York, NY, USA, 1988. [CrossRef]
34. Mason, W.P.; Baerwald, H. Piezoelectric Crystals and Their Applications to Ultrasonics. *Phys. Today* **1951**, *4*, 23–24. [CrossRef]
35. Berlincourt, D.; Krueger, H.H.A. Domain Processes in Lead Titanate Zirconate and Barium Titanate Ceramics. *J. Appl. Phys.* **1959**, *30*, 1804–1810. [CrossRef]
36. Stewart, M.; Cain, M.G. Direct Piezoelectric Measurement: The Berlincourt Method. In *Characterisation of Ferroelectric Bulk Materials and Thin Films*; Springer Series in Measurement Science and Technology: New York, NY, USA, 2014; pp. 37–64.
37. Perdew, J.P.; Burke, K.; Ernzerhof, M. Generalized Gradient Approximation Made Simple. *Phys. Rev. Lett.* **1996**, *77*, 3865–3868. [CrossRef]
38. Kresse, G.; Furthmuller, J. Efficient iterative schemes for ab initio total-energy calculations using a plane-wave basis set. *Phys. Rev. B* **1996**, *54*, 11169–11186. [CrossRef]
39. Kresse, G.; Joubert, D. From ultrasoft pseudopotentials to the projector augmented-wave method. *Phys. Rev. B* **1999**, *59*, 1758–1775. [CrossRef]
40. Lefki, K.; Dormans, G.J.M. Measurement of Piezoelectric Coefficients of Ferroelectric Thin-Films. *J. Appl. Phys.* **1994**, *76*, 1764–1767. [CrossRef]
41. Guo, Q.; Cao, G.Z.; Shen, I.Y. Measurements of Piezoelectric Coefficient d_{33} of Lead Zirconate Titanate Thin Films Using a Mini Force Hammer. *J. Vib. Acoust.* **2013**, *135*, 011003. [CrossRef]

42. Zhang, H.; Wang, Y.; Wang, L.; Liu, Y.; Chen, H.; Wu, Z. Process Control Monitor (PCM) for Simultaneous Determination of the Piezoelectric Coefficients d_{31} and d_{33} of AlN and AlScN Thin Films. *Micromachines* **2022**, *13*, 581. [CrossRef] [PubMed]
43. Matloub, R.; Hadad, M.; Mazzalai, A.; Chidambaram, N.; Moulard, G.; Sandu, C.S.; Metzger, T.; Muralt, P. Piezoelectric $Al_{1-x}Sc_xN$ thin films: A semiconductor compatible solution for mechanical energy harvesting and sensors. *Appl. Phys. Lett.* **2013**, *102*, 152903. [CrossRef]
44. Ruiz, E.; Alvarez, S.; Alemany, P. Electronic structure and properties of AlN. *Phys. Rev. B Condens. Matter* **1994**, *49*, 7115–7123. [CrossRef] [PubMed]
45. Wright, A.F. Elastic properties of zinc-blende and wurtzite AlN, GaN, and InN. *J. Appl. Phys.* **1997**, *82*, 2833–2839. [CrossRef]
46. Tsubouchi, K.; Mikoshiba, N. Zero-Temperature-Coefficient Saw Devices on Aln Epitaxial-Films. *IEEE Trans. Sonics Ultrason.* **1985**, *32*, 634–644. [CrossRef]
47. Mayrhofer, P.M.; Euchner, H.; Bittner, A.; Schmid, U. Circular test structure for the determination of piezoelectric constants of $Sc_xAl_{1-x}N$ thin films applying Laser Doppler Vibrometry and FEM simulations. *Sens. Actuator. A Phys.* **2015**, *222*, 301–308. [CrossRef]
48. Huang, Z.; Zhang, Q.; Corkovic, S.; Dorey, R.; Whatmore, R.W. Comparative measurements of piezoelectric coefficient of PZT films by Berlincourt, interferometer, and vibrometer methods. *IEEE Trans. Ultrason. Ferroelect. Freq. Contr.* **2006**, *53*, 2287–2293. [CrossRef]
49. Fialka, J.; Benes, P. Comparison of methods of piezoelectric coefficient measurement. In Proceedings of the 2012 IEEE International Instrumentation and Measurement Technology Conference Proceedings, Graz, Austria, 13–16 May 2012; pp. 37–42. [CrossRef]

Disclaimer/Publisher's Note: The statements, opinions and data contained in all publications are solely those of the individual author(s) and contributor(s) and not of MDPI and/or the editor(s). MDPI and/or the editor(s) disclaim responsibility for any injury to people or property resulting from any ideas, methods, instructions or products referred to in the content.